ISSN 0023-1584, Kinetics and Catalysis, 2011, Vol. 52, No. 2, pp. 316–329. © Pleiades Publishing, Ltd., 2011.
Original Russian Text © V.A. Radzig, A.A. Ischenko, 2011, published in Kinetika i Kataliz, 2011, Vol. 52, No. 2, pp. 325–339.

Carbon in Silica

V. A. Radzig[a] and A. A. Ischenko[b]

[a] *Semenov Institute of Chemical Physics, Russian Academy of Sciences, Moscow, 119991 Russia*
[b] *Lomonosov State Academy of Fine Chemical Technology, Moscow, 117571 Russia*
e-mail: radzig@chph.ras.ru

Received December 6, 2009

Abstract—The structure of paramagnetic centers (PMC) in carbon-doped silica is studied by the EPR and quantum chemistry methods. Three types of radicals, ≡Si–$^{\bullet}$CH$_2$, (≡Si–)$_2^{\bullet}$CH and (≡Si–)$_3$C$^{\bullet}$, are identified in which the free valence is localized on the impurity carbon atom. Their structure is determined by using samples enriched by isotopes ^{2}D, ^{29}Si, and ^{13}C. The assignment of the obtained radiospectroscopic parameters of radicals is confirmed by quantum-chemical calculations of model systems. Based on the obtained data, a conclusion is made that paramagnetic centers (the so-called EX-centers) discovered earlier by the EPR method in silicon oxidation products have the structure (≡Si-)$_3$C$^{\bullet}$, i.e. are not the intrinsic defects of the material but are related to impurity carbon atoms. Differences in the spectral characteristics of the (≡Si–)$_3$C$^{\bullet}$ groups observed in experiments are caused by the amorphous structure of silica. The kinetic nonequivalence of the (≡Si–)$_3$C$^{\bullet}$ radicals in the reaction of the hydrogen atom detachment from the H_2 molecule is established (the activation energies for different PMC fractions lie in the range from 10 to 17 kcal/mol). The quantum-chemical calculations of model systems performed in the paper suggest that the differences observed in the reactivity of radicals are related to their spatial structure. It is found that the high-temperature pyrolysis of the (≡Si–)$_3$C–H and (≡Si–O–)$_3$Si–H groups is accompanied by the quantitative regeneration of free radicals (≡Si–)$_3$C$^{\bullet}$ and (≡Si–O–)$_3$Si$^{\bullet}$. The probable mechanism of carbon atom embedding from. (≡Si–O–)$_3$Si–O–CH$_3$ groups to silica accompanied by the formation of (≡Si–)$_4$C groups is analyzed.

DOI: 10.1134/S0023158411010149

INTRODUCTION

The physicochemical characteristics of silica (amorphous SiO_2) are closely related to the nature of defects present in the material. These can be both intrinsic defects, in which silicon or oxygen atoms occur in states with unusual coordination, and groups containing impurity atoms. Their occurrence manifests itself in the spectroscopic characteristics of the material, especially, optical characteristics. As a rule, these centers initiate the chemical modification of glass structure in the development of new devices and accessories based on SiO_2, including fiber-optic system components [1].

In this work, we report the structure and properties of silica defects, whose constituents are carbon atoms as impurity atoms. The test material was reactive silica (RSi) [2, 3]—the product of the high-temperature (above 1000 K) vacuum pyrolysis of highly dispersed SiO_2 (Aerosil) whose surface ≡Si–O–H groups are converted into ≡Si–O–CH_3 groups as a result of methoxylation [2, 4]. The presence of carbon in pyrolysis products follows from IR-spectroscopic data [3, 4], and it was supported by the results of chemical analysis—the formation of CO_2 molecules on keeping RSi samples in an atmosphere of O_2 ($T > 750$ K) [5].

In this work, we used EPR and quantum-chemistry methods to analyze the structure of paramagnetic centers (PMCs) formed in the course of formation of RSi samples; the C atom was a constituent of these centers. Data on the structure and properties of these centers in silica were used in the discussion of their possible mechanisms of formation.

EXPERIMENTAL

The experiments were performed with highly dispersed powders of Aerosil A300 (the initial specific surface area was about 300 m^2/g). In particular experiments, a sample of silica enriched in the ^{29}Si isotope (65%; specific surface area of about 100 m^2/g) was used. The procedure of the thermochemical activation of a silica surface, which resulted in a dramatic increase in its chemical activity (the formation of so-called reactive silica (RSi)), was developed by Morterra and Low [2, 3]. It consisted of the two main stages: (1) silica surface methoxylation ($T = 700$ K; $P = 100$ Torr; $t = 15$ min; methanol of various isotopic compositions—CH_3OH, CD_3OD, and $^{13}CH_3OH$—was used (the carbon isotope content was about 80%)) and (2) high-temperature (up to 1300–1400 K) vacuum pyrolysis, which was accompanied by the degradation of methoxy groups and the formation of silyl hydride groups, the subsequent thermal decomposition of which resulted in the formation of RSi [3, 6].

A cell with the studies sample was connected with a high-vacuum system; this allowed us to perform experiments in a controlled atmosphere. The pressure of gases and vapors in the system was monitored using a Pirani gauge.

The EPR spectra of the samples were measured on an X-band EPR-20 IKhF instrument at 300 or 77 K.

The quantum-chemical calculations were performed using the Gaussian 94 software [7]. The fluorine-substituted molecular models of silica defects, in which ≡Si–O– groups were replaced by F atoms, were used in the calculations. For example, the $F_3Si–{}^{\bullet}CH_2$ radical served as a model of the $(≡Si–O–)_3Si–{}^{\bullet}CH_2$ radical. Radzig [6, 8] found that various types of paramagnetic and diamagnetic intrinsic and impurity defects in silica and their fluorine-substituted low-molecular-weight analogs have similar physicochemical characteristics. The reasons for this similarity are due to the spatial localization of electronic states at a defect atom and the fact that the F atom and the ≡Si–O– group as substituents have a similar effect on the properties of the silicon atom bound to them. The geometry of model's structures was optimized using a gradient procedure based on the density functional theory (DFT at the UB3LYP/6-311G(*d*,*p*) level [9, 10]). Vibrational spectra (for all of the optimized structures), and radiospectroscopic parameters (for paramagnetic species) were calculated. The energetics of individual structures was refined by single-point calculations at the G2(MP2)/B3LYP/6-311G** level [11].

In the study of the reactivity of PMCs, it is desirable to use a sample containing controlled amounts of free radicals of certain types. The main part of PMCs, which are stabilized on the surface of the RSi samples are $(≡Si–O–)_3Si^{\bullet}$ radicals [6, 12]. For the passivation of these centers, the following reaction sequence with gas-phase molecules was used [6, 12]:

$$(≡Si–O–)_3Si^{\bullet} + N_2O \longrightarrow (≡Si–O–)_3Si–O^{\bullet} + N_2,$$

$$(≡Si–O–)_3Si–O^{\bullet} + H_2 \longrightarrow (≡Si–O–)_3Si–O–H + H,$$

$$(≡Si–O–)_3Si–O^{\bullet} + H \longrightarrow (≡Si–O–)_3Si–O–H.$$

The resulting hydroxyl groups were thermally stable toward homolytic decomposition reactions (the strength of the O–H bond is about 125 kcal/mol, and the strength of the Si–O bond is even higher).

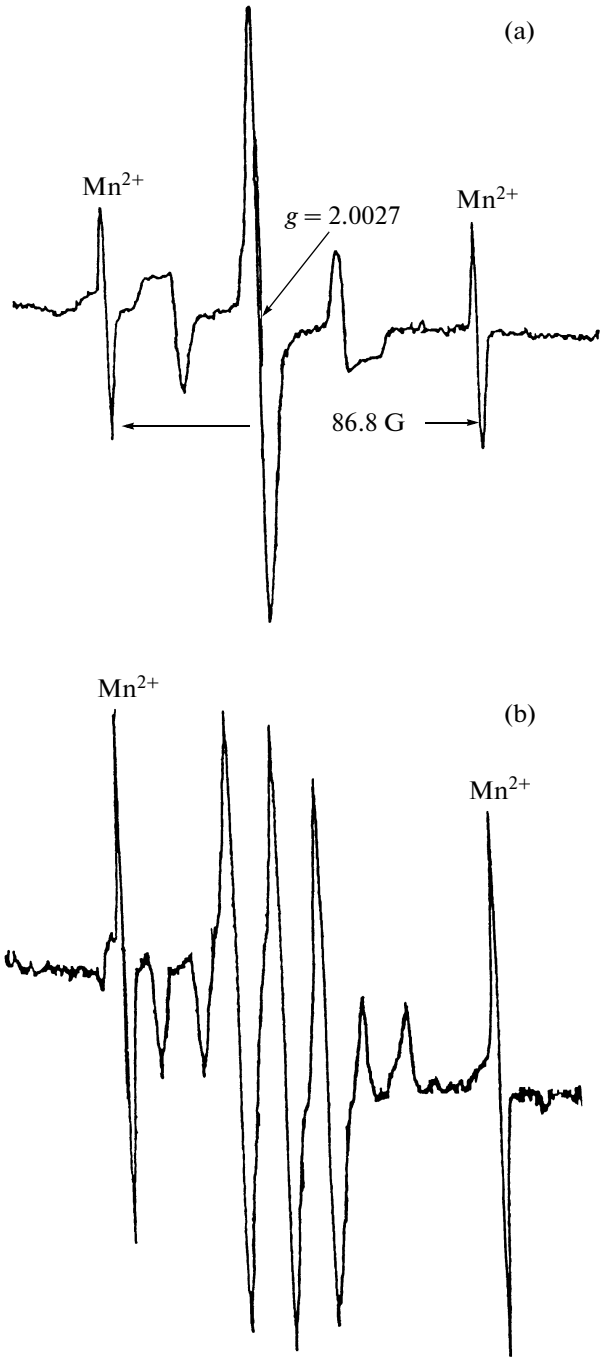

Fig. 1. EPR spectra of $≡Si–{}^{\bullet}CH_2$ radicals (T = 300 K): (a) $≡{}^{28}Si–{}^{\bullet}CH_2$ and (b) $≡{}^{28}Si–{}^{\bullet}CH_2$ (35%) + $≡{}^{29}Si–{}^{\bullet}CH_2$ (65%).

RESULTS AND DISCUSSION

1. ≡Si–$^{\bullet}$CH$_2$ radical. The heating of a methoxylated silica sample at 900 K was accompanied by the formation of PMCs, the EPR spectrum of which is shown in Fig. 1a. It is a triplet with g = 2.0026. The measurement of an EPR signal at 77 K did not considerably change its shape. The edge components of a triplet signal have an anisotropic shape, whereas the central component is a single narrow line. The line intensity ratio is close to 1 : 2 : 1. This suggests that the hyperfine structure (HFS) of the observed EPR signal was due to the interaction of an unpaired electron with two magnetically equivalent nuclei with spins of 1/2 and had the parameters $a_{\parallel} = 26 \pm 0.5$ G, $a_{\perp} = 18.5 \pm 0.5$ G, and $a_{iso} = 21.0 \pm 0.5$ G. The isotropic component of hyperfine coupling (HFC) tensors was typical of α protons, the constituents of free-radical $>C^{\bullet}–H$ groups [13].

Table 1. Radiospectroscopic parameters of carbon-centered radicals

Entry	Radical	Nucleus	a_{iso}	b_1	b_2	b_3	Nucleus	a_{iso}	b_1	b_2	b_3	Nucleus	a_{iso}	b_1	b_2	b_3
1	$\equiv Si-\dot{C}H_2$	^1H	−21.0	−5.0	2.5	2.5	^{29}Si	21.0								
2	$F_3Si-\dot{C}H_2$	^1H	−20.6	−13.2	−0.8	14.0	^{29}Si	21.3	1.5	0.8	−2.4	^{13}C	22.7	−26.2	−26.1	52.3
3	$F_3Si-\dot{C}H_2$*	^1H	−20.6	−8.0	4.0	4.0	^{29}Si	21.3	1.5	−0.7	−0.7	^{13}C	22.7	−26.2	13.1	13.1
4	$(\equiv Si-)_2\dot{C}H$	^1H	−17.3	−8.5	−0.6	9.1										
4a	$a_1(H,(D)) = -8.8(-1.3)$; $g_1 = 2.0024$; $a_2(H,(D)) = 16.8(2.6)$; $g_2 = 2.0028$; $a_3(H,(D)) = -26.4(-4.1)$; $g_3 = 2.0030$															
5	$(F_3Si-)_2\dot{C}H$	^1H	−18.8	−12.5	−0.8	13.3	^{29}Si	18.8	1.1	0.5	−1.6	^{13}C	20.7	−24.9	−24.8	49.7
6	$(\equiv Si-)_3C^{\cdot}$	–	–	–	–	–	^{29}Si	16.1	<1	<1	<1	^{13}C	23.2	−23.2	−23.2	46.4
7	$(F_3Si-)_3C^{\cdot}$	–	–	–	–	–	^{29}Si	16.7	0.8	0.3	−1.1	^{13}C	19.4	−23.8	−23.8	47.5

Note: Entries 1, 4, and 6 refer to experimental results; entries 2, 3, 5, and 7 refer to the results of calculations; b_i are the main components of an anisotropic HFC tensor; all of the values are expressed in G.
* The result of calculations based on a model of free single-axis rotation about the Si–C bond in the radical.

In the sample of silica enriched in the ^{29}Si isotope ($I = 1/2$; 65%), the EPR spectrum was a superposition of two signals (Fig. 1b). One of them coincided with that shown in Fig. 1a. The second spectrum differs from the first in that each triplet component is additionally split into a doublet of 20.5 ± 0.5 G. The intensity of the second signal is 65% of the total intensity of the spectrum; that is, the doublet splitting is related to the interaction of an unpaired electron with the ^{29}Si nucleus in the radical.

The above experimental data suggest that the observed EPR signal belongs to $\equiv Si-\dot{C}H_2$ radicals, and its HFS determinate by the interaction of an unpaired electron with two magnetically equivalent α protons and a silicon atom. The axially symmetrical shape of HFC tensors with protons was due to the fact that, even at 77 K, the free rotation of a methylene group about the Si–C bond was unfrozen. Table 1 summarizes the radiospectroscopic parameter of the radical (entry 1).

Figure 2a shows the optimized structure of the $F_3Si-\dot{C}H_2$ radical–the molecular model of a surface site. The calculated values of HFC tensors of an unpaired electron with magnetic nuclei in the radical are given in Table 1 (entry 2). In this case, the interaction of an unpaired electron with the atomic nucleus of silicon is mainly isotropic. Thus, the experimentally observed radiospectroscopic parameters of the $\equiv Si-\dot{C}H_2$ radical are in concordance with the results of calculations for an accepted molecular model of a surface center.

According to the results of calculations, the height of a barrier for the rotation of a methylene group in the $F_3Si-\dot{C}H_2$ radical was lower than 1 kcal/mol; consequently, its rotation frequency at 77 K was no lower than 10^{10} s^{-1}. It can be considered as free rotation on a scale of frequencies affecting the shape of the EPR spectrum of the radical. The main components of axially symmetrical HFC tensors calculated for the methylene group freely rotating about the Si–C bond in the $F_3Si-\dot{C}H_2$ radical are given in Table 1 (entry 3). A comparison of calculated (Table 1, entry 3) and experimentally observed (Table 1, entry 1) values indicates that the model of the rapid single axis rotation of the methylene group about the Si–C bond is deficient. It should be hypothesized that other types of displacement occur to cause the effective averaging of the HFC tensor anisotropy of an unpaired electron with protons.

Upon the contact of a sample containing $\equiv Si-\dot{C}H_2$ radicals with oxygen, its EPR spectrum changed. This means that the radical is accessible to environmental molecules; that is, it is stabilized on a solid surface. Bobyshev and Radtsig [14] found that the peroxide radical formed by the addition of an oxygen molecule underwent isomerization even at 300 K with the release of a formaldehyde molecule:

$$\equiv Si-\dot{C}H_2 + O_2 \longrightarrow \equiv Si-CH_2-O-O^{\cdot}$$
$$\longrightarrow \equiv Si-O^{\cdot} + CH_2=O.$$

2. $(\equiv Si-)_2\dot{C}H$ radical. As the temperature of pyrolysis was increased (above 1000 K), the concentration of PMCs in the sample increased and the shape of their EPR spectrum changed (Fig. 3, spectra *1* and *4* (solid line)). Anisotropic lines arranged at the wings of the EPR spectrum belong to a new PMC (the central line in spectrum *4* (solid line) in Fig. 3 is due to the presence of other types of PMCs in the sample:

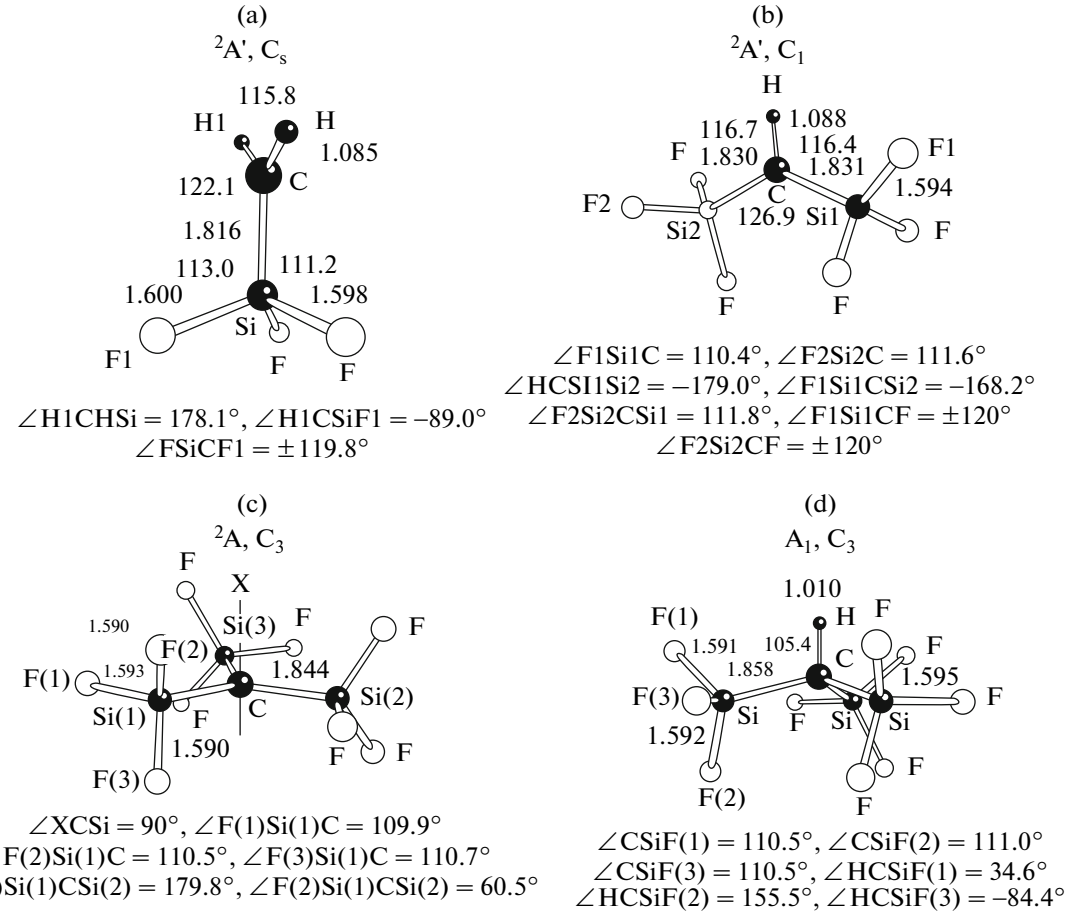

Fig. 2. Optimized structures of (a) $F_3Si-{}^{\bullet}CH_2$, (b) $(F_3Si-)_2{}^{\bullet}CH$, (c) $(F_3Si-)_3C^{\bullet}$, and (d) $(F_3Si-)_3CH$.

$(\equiv Si-O-)_3Si^{\bullet}$ [5, 6] and $(\equiv Si-)_3{}^{12}C^{\bullet}$ radicals (see Section 3)).[1]

Using CD_3-OD as a methylating agent, we can dramatically change the shape of the EPR spectrum of the detected signal (Fig. 3, spectrum *4* (dashed line)): it is changed to an anisotropic triplet in place of an anisotropic doublet. Therefore, the observed HFS was due to the interaction of an unpaired electron with a proton ($I = 1/2$) or deuteron ($I = 1$). Table 1 summarizes the principal components of *a* and *g* tensors (the signs of *a*-tensor components were taken from quantum-chemical calculations (see below)). The isotropic components of these tensors are $a_{iso}(H) = 17.3 \pm 0.2$ G, $a_{iso}(D) = 2.7 \pm 0.05$ G, and $g_{iso} = 2.0027 \pm 0.0001$. A change in the temperature of EPR-spectroscopic measurements over a range of 77–300 K did not result in noticeable variations in the shapes of observed signals.

Figure 3 (curve *2*) shows a calculated EPR spectrum of the radical whose spin Hamiltonian parameters (*a* and *g* tensors) were taken from Table 1 (entry 4a) and the Zeeman proton energy was taken into account in the second order of perturbation theory (the program for calculations was provided by A.Kh. Vorob'ev (Moscow State University)). It can be seen that the shapes of experimentally observed and calculated EPR signals were consistent. For comparison, Fig. 3 (curve *3*) shows the calculated spectrum of a radical with the same spin Hamiltonian but without consideration for a term responsible for the Zeeman proton energy. Thus, the unusual shape of a parallel component (g_1, a_1) of the EPR spectrum of the $\equiv{}^{28}Si-H^{12}C^{\bullet}-{}^{28}Si\equiv$ radical (Fig. 3, spectrum *1*) was due to the fact that the constant a_1 was close to the distance between the Zeeman levels for a proton in a magnetic field of 3450 G (about 10.5 G), and transitions with the simultaneous overturn of electron and proton spins (forbidden transition) should be taken

[1] The contribution from $(\equiv Si-O-)_3Si^{\bullet}$ radicals to the detected EPR signal can be decreased many times by converting these radicals into another species, for example, peroxide, which has a much broader EPR spectrum [15]. The EPR spectrum of the $(\equiv Si-)_3{}^{12}C^{\bullet}$ radical is a single narrow line (see below) arranged in the region of magnetic fields where the $\equiv{}^{28}Si-H^{12}C^{\bullet}-{}^{28}Si\equiv$ radical (unlike $\equiv{}^{28}Si-D^{12}C^{\bullet}-{}^{28}Si\equiv$) does not exhibit intense absorption lines.

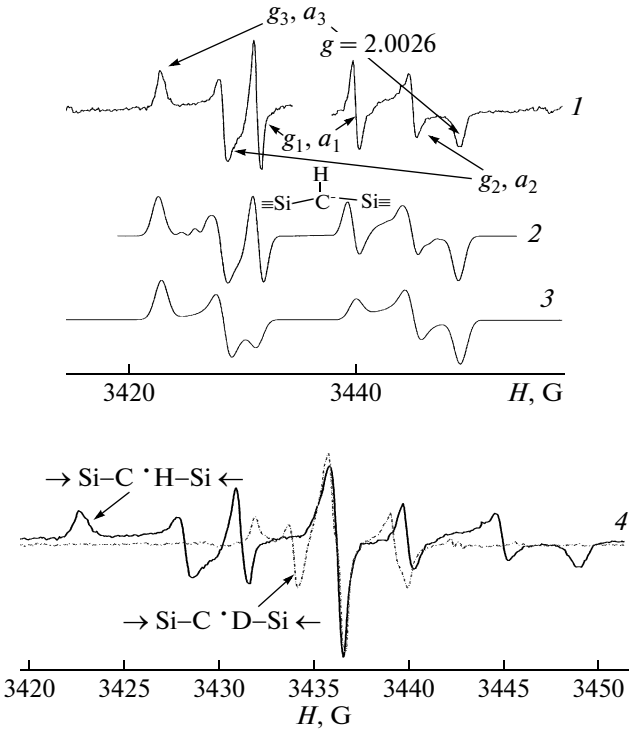

Fig. 3. EPR spectra of ≡Si–HC˙–Si≡ and ≡Si–DC˙–Si≡ radicals (300 K): (*1*) ≡Si–HC˙–Si≡; (*2, 3*) the EPR spectra of the radical whose spin-Hamiltonian parameters are given in Table 1 (entry 4a) calculated based on second-order perturbation theory (*2*) with consideration of the Zeeman proton energy and (*3*) without this term; and (*4*) ≡Si–HC˙–Si≡ (solid line) and ≡Si–DC˙–Si≡ (dashed line).

into account in the shape analysis of the EPR spectrum of this radical.

In the order of radicals $H_2C^{\cdot}-H$, ≡Si–HC˙–H, and ≡Si–HC˙–Si≡, the isotropic HFC constants of an unpaired electron with the **α** proton were –23 [13], –21.0, and –17.3 G, respectively (see Table 1). Consequently, upon the replacement of the **α**-H atom by a group containing the Si atom, the isotropic HFC constants of an unpaired electron with the **α** proton decreased by 2–3 G.

An anisotropic character of the EPR spectra of these centers was retained upon the measurement of the signal over a broad temperature range of 77–300 K. This fact suggests that the amplitude of C and H(D) atom displacements of a radical fragment with respect to an equilibrium position was small; that is, the C atom was bound to immobile atoms of a solid, which fixed its spatial position. These atoms in the structure of silica are tetracoordinated silicon atoms.

Figure 2b shows the equilibrium (optimized) geometry of a molecular model of the ≡Si–HC˙–Si≡ center—the $F_3Si-HC^{\cdot}-SiF_3$ radical. Table 1 (entry 5) summarizes the DFT-calculated components of the HFC tensor of an unpaired electron with magnetic nuclei in this radical. They are consistent with the experimentally determined values for the ≡Si–HC˙–Si≡ radical.

The HFC constants of an unpaired electron with ^{13}C and ^{29}Si in the ≡Si–HC˙–Si≡ radical were not determined experimentally. However, we believe that they are close to the values calculated for the $F_3Si-HC^{\cdot}-SiF_3$ radical (see Table 1). Indeed, they were mutually consistent in the cases when the experimentally measured and calculated values of corresponding constants could be compared (for the ^{29}Si nucleus in radicals like ≡Si–˙CH_2 (entries 1 and 2 in Table 1) and with ^{13}C and ^{29}Si nuclei in $(\equiv Si-)_3C^{\cdot}$ radicals (entries 6 and 7 in Table 1)).

Using the results of calculations, we can determine the orientation of the main *g*-tensor axes in the radical. As expected, the component $g_2 = 2.0024$, which is the closest in value to the *g*-factor of free electron (2.0023), was oriented along the 2*p*-AO axis of the carbon atom, at which an unpaired electron was localized. This situation is typical of alkyl-type radicals: in this direction, the action of the spin–orbital interaction operator, which leads to a *g*-factor shift as a result of admixing excited electronic states to the wave function of the electronic ground state, reaches a minimum, and the corresponding *g*-tensor component is close to its value for a free electron. The *g*-tensor component ($g_3 = 2.0030$) oriented along the C–H bond of the radical underwent the greatest shift.

3. $(\equiv Si-)_3C^{\bullet}$ radical. Figure 4a (spectrum *1*) shows the EPR spectrum of an RSi sample after activation at 1350 K. It is a superposition of signals from two radicals. The anisotropic line, whose shape depends on an axially symmetrical *g* tensor ($g_{\parallel} = 2.0018, g_{\perp} = 2.0003$), belongs to $(\equiv Si-O-)_3Si^{\cdot}$ radicals [5, 6]. This radical was converted into a peroxide species upon contact of the sample with oxygen. The EPR spectrum of peroxide radical has the width near 100 G and, as a result, low amplitude (see Section 2) [15]. The EPR spectrum of the second radical, which remained unchanged as a result of oxygen treatment at 300 K, is given in Fig. 4a (spectrum *2*). It is a narrow (~1 G), single symmetrical line with a *g*-factor of 2.0026. It will be demonstrated below that the observed signal belongs to $(\equiv Si-)_3C^{\cdot}$ radicals. The amounts of PMCs calculated from EPR-spectroscopic data were $(2.4 \pm 0.5) \times 10^{11}$ cm^{-2} ($(6 \pm 1) \times 10^{17}$ spin/g) for $(\equiv Si-O-)_3Si^{\cdot}$ radicals and $(2.5 \pm 0.5) \times 10^{10}$ cm^{-2} ($(6.2 \pm 1) \times 10^{16}$ spin/g) for $(\equiv Si-)_3C^{\cdot}$ radicals. Note that the ratio between the amounts of PMCs noticeably changed (by a factor of a few) depending on RSi sample preparation conditions (especially, the final temperature and the rate of sample heating (the rate of pyrolysis)).

The EPR signal of $(\equiv Si-)_3C^{\cdot}$ radicals became saturated at low microwave power levels. The presence of paramagnetic oxygen molecules in a gas phase over the sample affected the saturation. As the gas pressure was increased, the time of spin relaxation of PMCs decreased as a result of collisions with paramagnetic

oxygen molecules (spin exchange). This fact suggests that the centers were stabilized in a near-surface layer of silica. The oxygen effect in this system will be considered elsewhere.

In silica samples with natural isotope concentrations, the EPR spectrum of the $(\equiv Si-)_3C^{\bullet}$ radical always contained a pair of low-intensity satellite lines along with a central single line (Fig. 4b). They were symmetrically arranged with respect to the central line; the distance between them was 16.1 G, and their total intensity was about 15% of the total signal intensity.

The problem of the nature of the observed satellite lines was solved in experiments performed with a sample of silica enriched in the ^{29}Si isotope (65%). Figure 4c shows the EPR spectrum of this sample. It consists of seven equidistant lines with a distance of 8.05 G between them; it is a superposition of signals from centers containing various numbers of magnetically equivalent silicon nuclei ^{29}Si (from zero to three) with the isotropic constant $a_{iso}(^{29}Si) = 16.1$ G. The relative intensity of signals depends on the probability of the fact how many nuclei of this type are the constituents of a PMC.

The chemical nature of radicals was determined in experiments in which the RSi samples were performed with the use the silica with a natural concentration of the ^{29}Si isotope and CH_3OH enriched in the carbon isotope ^{13}C (the concentration of this isotope was 75–80%, I = 1/2). Figure 5a shows the EPR spectrum of radicals in this sample. It consists of a central portion, which is identical to that obtained previously for samples prepared with the use of ordinary methanol (Fig. 4b) in terms of signal shape (with consideration for satellite lines), and two new lines arranged at a distance of 70 G from each other.

Figure 5b shows the EPR spectrum in an integral form. In this case, its characteristic features are more clearly pronounced. First, note that the shape of the integral absorption line, which is a distribution function of magnetic field strength for the number of resonating spins, in the main portion (other than central) is nearly constant. This is most clearly pronounced in the high-field region of the spectrum. Small deviations from this dependence in the low-field region of the spectrum are due to the overlapping of a signal from PMCs of another type ($(\equiv Si-O-)_3Si-O-O^{\bullet}$ peroxide radicals) in this sample. In Fig. 5b, a dashed integral absorption line is separated into two portions. We will demonstrate below that this corresponds to the separation of EPR signals from $(\equiv Si-)_3{}^{12}C^{\bullet}$ radicals in the top portion of the spectrum and from $(\equiv Si-)_3{}^{13}C^{\bullet}$ radicals in the bottom portion of the spectrum. The ratio between surface areas under these curves is 0.2 : 1, which is close to the degree of enrichment of the used methanol in the ^{13}C isotope. Thus, the above experimental results suggest that the carbon atom is a constituent of a PMC.

Figure 2c shows the optimized structure of the $(F_3Si-)_3C^{\bullet}$ radical. Table 1 (entry 6) summarizes the

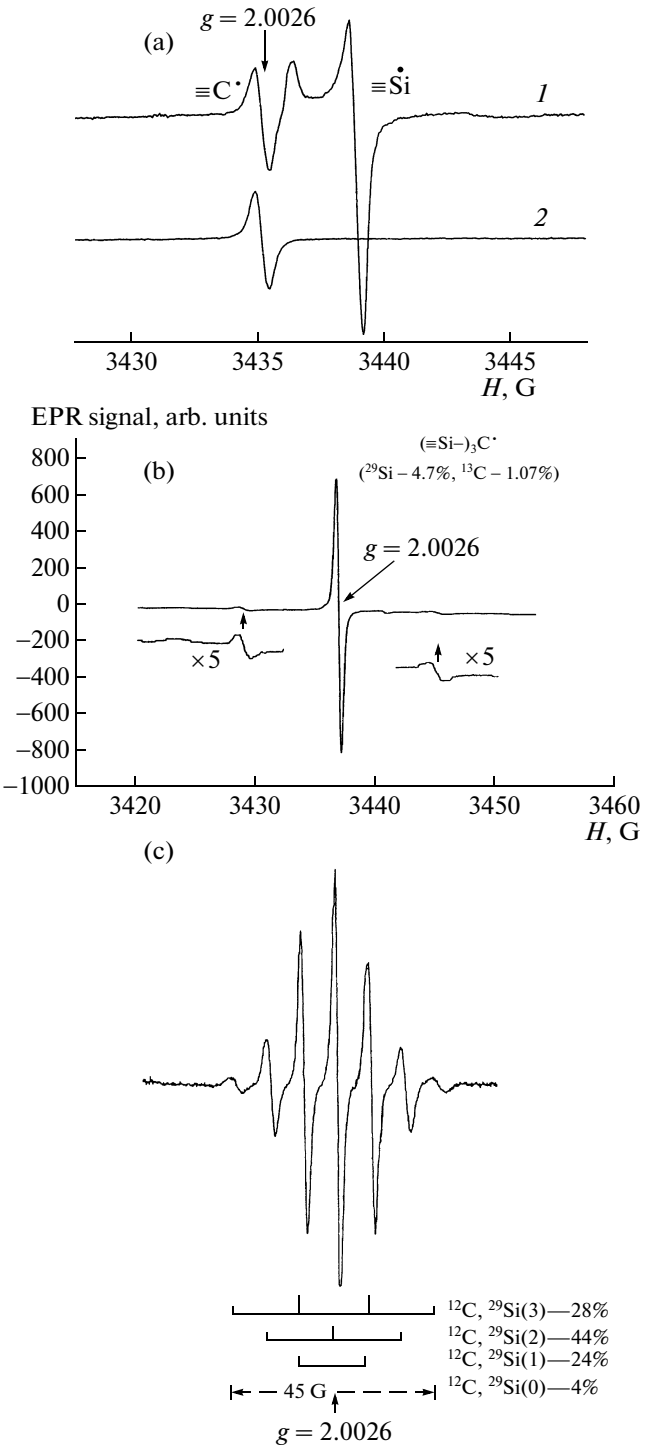

Fig. 4. EPR spectra of (a) radicals in the RSi sample (T = 300 K) (*1*) before and (*2*) after the chemisorption of O_2 at room temperature, (b) the $(\equiv Si-)_3{}^{12}C^{\bullet}$ radical (4.7% ^{29}Si), and (c) the $(\equiv Si-)_3{}^{12}C^{\bullet}$ radical (65% ^{29}Si).

DFT-calculated HFC constants with ^{13}C and ^{29}Si nuclei and spin densities on these nuclei in the radical. According to the results of the calculations, the main portion of spin density (0.97) in the radical is localized

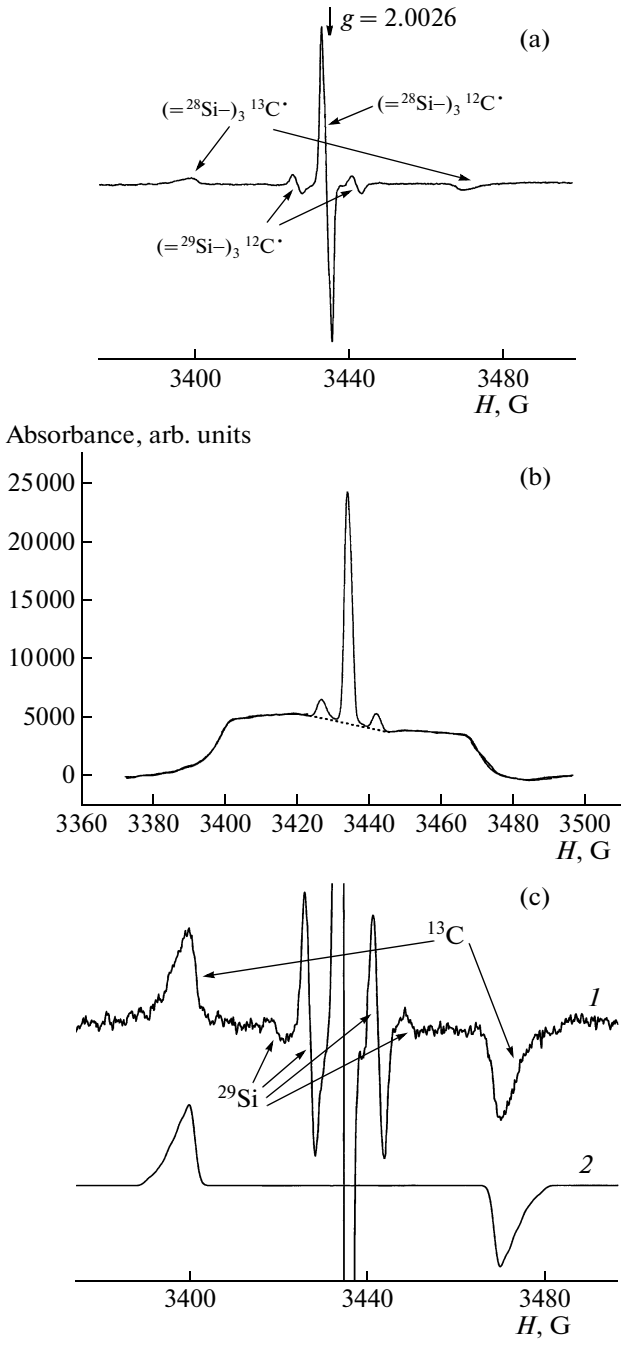

Fig. 5. EPR spectra of $(\equiv Si-)_3C^{\bullet}$ radicals (4.7% ^{29}Si; 80% ^{13}C; $T = 300$ K): (a) as an absorption derivative, (b) in an integral form, (c) (*1*) a signal detected at a high level of amplification, and (*2*) a calculated spectrum (for details, see the text).

at the carbon atom. The HFC tensor with the ^{13}C nucleus is axially symmetrical; the parallel tensor component is about 70 G, whereas the perpendicular component is close to zero. Note that the experimental and calculated (for the PMC model) HFC constants for an unpaired electron with ^{29}Si nuclei in the radical are close to each other. Thus, the results of calculations support the conclusion that the test radical has the $(\equiv Si-)_3C^{\bullet}$ structure.

The unusual shape of the EPR spectrum of the $(\equiv Si-)_3{}^{13}C^{\bullet}$ radical (Fig. 5b) was due to a specific form of the axially symmetrical HFC tensor of an unpaired electron with the ^{13}C nucleus, which had a nonzero ($a_1 \cong 70$ G) and two near-zero ($a_2 = a_3 \cong 0$) principal components. With this HFC tensor, the positions of lines in the EPR spectrum is determined from the simple relationship $(H-H_0) = a_1\cos\theta$, where θ is the angle between the direction of an external magnetic field (H) and the orientation of the radical symmetry axis in the sample. At an equally probable orientation of axes (powder), the intensity of microwave power absorption by the sample is proportional to $d(\cos\theta)/dH$. As a result, the distribution function of the number of spins resonating in the field with intensity H is independent of H (see Fig. 5b).

A line shape in the region of parallel components of well-resolved EPR spectra is the integral shape of an individual line [16]. In the EPR spectrum of the $(\equiv Si-)_3{}^{13}C^{\bullet}$ radical, the corresponding components are asymmetric (Fig. 5c, spectrum *1*) with tails toward a side from the center of the signal. The observed asymmetry was due to difference in the component $a_{\parallel}$ of the HFC tensor of an unpaired electron with the ^{13}C nucleus for individual groups of $(\equiv Si-)_3{}^{13}C^{\bullet}$ radicals. Figure 5c (spectrum *2*) shows the simulated EPR spectrum as a superposition of five signals with different values of $a_{\parallel}$ = 69.5 (0.8), 74 (0.6), 78.5 (0.4), 83 (0.2), and 87.5 (0.1) G and $a_{\perp} = 0$ (the figures in parentheses indicate the weights of corresponding radical fractions). It can be seen that the experimental and calculated spectra are consistent.

Differences in the radiospectroscopic characteristics of individual groups of radicals suggest differences in their geometric structures. For carbon-containing radicals, the HFC constants for the central C atom at which an unpaired electron is localized depend on the character of hybridization of its wave function. In turn, this wave function depends on the deviation of the C atom from a plane formed by its three nearest substituents; the angle φ is taken as a measure of this deviation (see Fig. 6) [13, 16]. Figure 6a shows the φ-angle dependences of the energies of the $(F_3Si-)_3C^{\bullet}$ radical (curve *1*) and the $(F_3Si-)_3C-H$ molecule (*2*), as calculated using quantum-chemical methods (DFT level), whereas Fig. 6b shows the radiospectroscopic characteristics of the radical, HFC constants of an unpaired electron with the ^{13}C nucleus ($a_{iso}(^{13}C)$, curve *1* and $-b_1(^{13}C)$, curve *2*) and the ^{29}Si nucleus ($a_{iso}(^{29}Si)$, curve *3*). The geometries of the molecule and the radical were varied with the conservation of their spatial symmetry (C_{3v}), and the other geometry parameters of the molecule and the radical were optimized at a fixed φ angle. A planar configuration of the radical ($\varphi = 90°$) (curves *1*) corresponds to a minimum radical energy and a minimal value of the paral-

lel component of the HFC tensor with the ^{13}C nucleus. An increase in the degree of pyramidality of the radical structure (an increase in φ angle) resulted in an increase in the energy of the system. Simultaneously, the parallel component of the HFC tensor changed—it increased due to an increase in the isotropic component, whereas anisotropic tensor components and HFC constants with ^{29}Si nuclei in the radical changed only slightly (the interaction with the ^{29}Si nucleus was mainly isotropic). A comparison of the results of calculations with experimental data allowed us to conclude that the $(\equiv Si-)_3C^{\bullet}$ radicals stabilized in an amorphous silica matrix differ in the degrees of pyramidality, and the characteristic value of φ angle lies in a range from 90° (planar structure) to 100°.

4. Reactivity of $(\equiv Si-)_{3-n}C^{\bullet}H_n$ ($n = 0$, 1, or 2) and $(\equiv Si-O-)_3Si^{\bullet}$ radicals toward H_2 molecules. In this section, we report the results of a study of the reactivity of detected free radicals. Hydrogen belongs to a few gases that are soluble in SiO_2 under comparatively mild conditions. Thus, it is used to modify the structure of glass. We studied the reactions of carbon- and silicon-centered radicals with molecular hydrogen and the reverse reactions of homolytic C–H and Si–H bond cleavage:

$$(\equiv Si-O-)_3Si^{\bullet} + H_2 \longrightarrow TS \longrightarrow (\equiv Si-O-)_3Si-H + H, \quad (I)$$

$$(\equiv Si-O-)_3Si-H \longrightarrow (\equiv Si-O-)_3Si^{\bullet} + H, \quad (II)$$

$$(\equiv Si-)_{3-n}C^{\bullet}H_n + H_2 \longrightarrow TS \longrightarrow (\equiv Si-)_{3-n}C-H_{n+1} + H, \quad (III)$$

$$(\equiv Si-)_{3-n}C-H_{n+1} \longrightarrow (\equiv Si-)_{3-n}C^{\bullet}H_n + H, \quad (IV)$$

where TS is the transition state.

Data on the reactivity of radicals were obtained using EPR and quantum chemistry methods. The experimental results mainly belong to $(\equiv Si-O-)_3Si^{\bullet}$ (I) and $(\equiv Si-)_3C^{\bullet}$ (II) radicals, and model quantum-chemical calculations were performed for all types of the experimentally detected PMCs.

The RSi samples contained PMC of the following two types: $(\equiv Si-O-)_3Si^{\bullet}$ (I) and $(\equiv Si-)_3C^{\bullet}$ (II). This allowed us to compare their reactivity. First, the contact of this sample with hydrogen ($T = 295$ K) was accompanied by the decay of radicals (I) in reaction (I) (see also [17]). This process was complete more rapidly that noticeable changes in the concentration of radicals (II) occurred. Figure 7a shows the dependence of the concentration $N(t)$ of radicals (I) on the time of sample exposure in an atmosphere of hydrogen (pressure $P_{H_2} = 1.5$ Torr, $T = 295$ K). This dependence was nearly linear in the $\ln(N_0/N(t))-t$ coordinates. Thus, $N(t) = N_0\exp(-k_{eff}t)$. As determined from the slope of the straight line, $k_{eff} = k(295\text{ K})P_{H_2} = 2.45 \times 10^{-3}$ s^{-1} and the rate constant of reaction (I) is k (295 K) $= (6 \pm 1.5) \times 10^{-20}$ cm^3 molecule^{-1} s^{-1}, which is consistent with published data [17] (k (295 K) $= (8 \pm 1.5) \times 10^{-20}$ cm^3 molecule^{-1} s^{-1}). Specifying a preexponential factor of 10^{-11} cm^3 molecule^{-1} s^{-1} (see below), we can estimate the activation energy of reaction (I) at 11.2 kcal/mol.

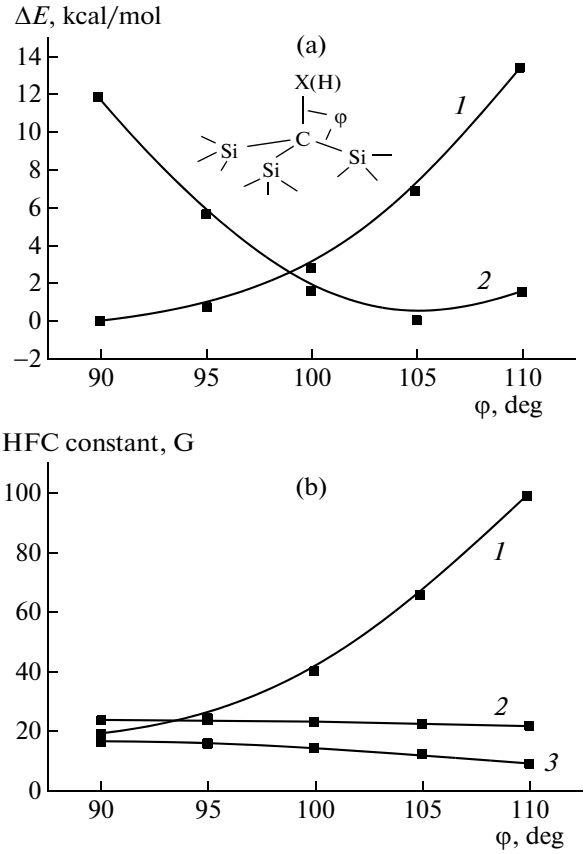

Fig. 6. Results of quantum-chemical calculations for (a) the dependence of the energies of (*1*) the $(F_3Si-)_3C^{\bullet}$ radical and (*2*) the $(F_3Si-)_3CH$ molecule on angle φ (C_{3v} symmetry) and (b) the dependence of HFC constants in the $(F_3Si-)_3C^{\bullet}$ radical on angle φ: (*1*) $a_{iso}(^{13}C)$, (*2*) $-b_1(^{13}C)$ (see Table 1), and (*3*) $a_{iso}(^{29}Si)$.

Let us consider the reaction of $(\equiv Si-)_3C^{\bullet}$ radicals with hydrogen (reaction (III)). As expected, the difference found in the spectroscopic (radiospectroscopic) characteristics of $(\equiv Si-O-)_3C^{\bullet}$ radicals also manifested itself in their kinetic behavior. Figure 7b shows the kinetic curve of decay at $T = 650$ K and $P_{H_2} = 2.5 \times 10^{-2}$ Torr. Unlike reaction (I), in which the participating PMCs are similar in reactivity, here, we are dealing with a process with the participation of kinetically nonequivalent centers (the case of so? called polychromatic kinetics) [18, 19]. The main characteristic responsible for the kinetics of this process is the distribution function of the number of radicals $n(k, 0)dk$, $n(k, t) = n(k, 0)\exp(-kt)$, and $N(t) =$

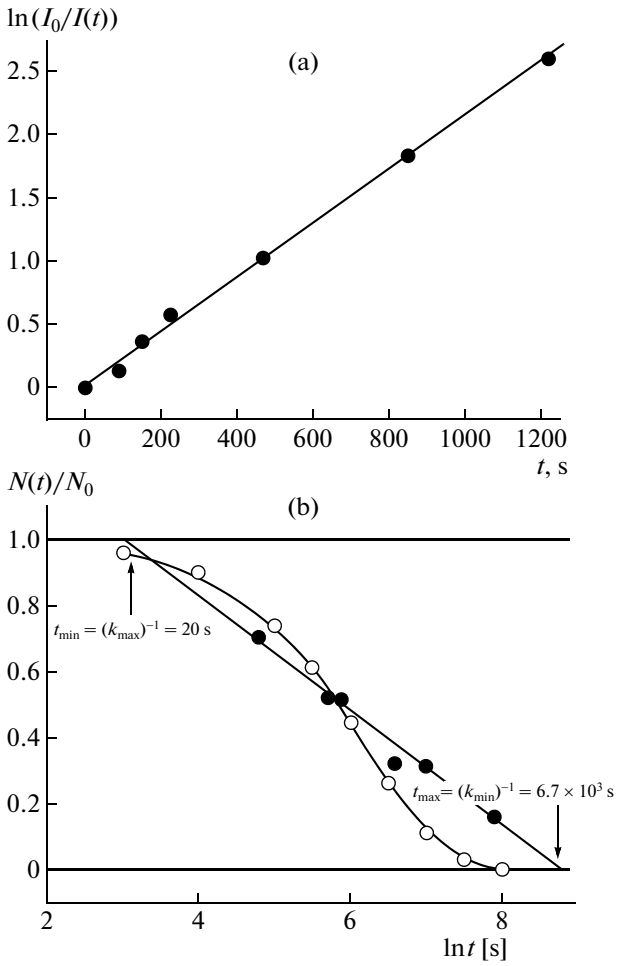

Fig. 7. Kinetic curves for the hydrogenation reactions of radicals: (a) $(\equiv Si{-}O{-})_3Si^{\bullet} + H_2 \longrightarrow (\equiv Si{-}O{-})_3Si{-}H + H$; $T = 295$ K; $P_{H_2} = 1.5$ Torr; (b) $(\equiv Si{-})_3C^{\bullet} + H_2 \longrightarrow (\equiv Si{-})_3C{-}H + H$; (*1*) $T = 650$ K; $P_{H_2} = 2.5 \times 10^{-2}$ Torr; (*2*) kinetic curve for a monochromatic reaction with the rate constant $kP^{|}{}_{H_2} = 2.1 \times 10^{-3}\ s^{-1}$.

$\int n(k, t)dk$ (it is believed that radicals do not transfer from one fraction to another in the course of the process). The simplest to analyze case is that a linear relationship between $(N(t)/N_0)$ and ln*t* takes place in the region of conversion of the main portion of reacting particles (from 20 to 80%) [18, 19]. Reaction (III) obeys this kinetics (see Fig. 7b). In this case, the distribution function takes the form $n(k, 0)dk \sim (1/k)dk$, $k_{min} \le k \le k_{max}$; that is, it depends of the parameters $k_{min} = 1/t_{max}$ and $k_{max} = 1/t_{min}$, and t_{min} and t_{max} are the *x* coordinates of the intersections of a linear anamorphosis of the kinetic curve with lines $y = 1$ and $y = 0$. Figure 7b shows how these parameters are determined from the shape of the kinetic curve: $k_{min} = 1/t_{max} = 1.5 \times 10^{-4}\ s^{-1} \le k \le k_{max} = 1/t_{min} = 4.9 \times 10^{-2}\ s^{-1}$, $k_{min} = k(0)_{min}\exp(-E_{max}/RT)\,P'_{H_2}$; and, analogously, $k_{max} = k(0)_{max}\exp(-E_{min}/RT)\,P'_{H_2}$, where $k(0)\exp(-E/RT)$ is the rate constant of the reaction of the radical with the hydrogen molecule in the Arrhenius form, P'_{H_2} is the concentration of dissolved hydrogen, which was assumed proportional to its concentration in a gas phase $P'_{H_2} = \alpha(H_2, T)\,P_{H_2}$ with the value of $\alpha(H_2, 650\ K) = 0.03$ [20].

Dissolved hydrogen takes part in reaction (III). In the case of a diffusion-controlled reaction, the rate constant is $k_D = 4\pi r_0 D$, where r_0 is the radius of trapping a diffusing molecule by the center. According to Shelby [20], the diffusion coefficient of hydrogen in amorphous SiO_2 is $D = 5.65 \times 10^{-4}\exp(-10.4\ (kcal/mol)/RT)\ cm^2/s$. Thus, the lifetime of a center into diffusion control reaction is

$$t_D = (k_D(650\ K)\,P'_{H_2})^{-1}$$
$$= (4\pi r_0 D(650\ K)\,P'_{H_2})^{-1}$$
$$= (4\pi(5 \times 10^{-8}\ cm)(1.8 \times 10^{-7}\ cm^2/s) \times (1.1 \times 10^{13}\ cm^{-3}))^{-1} = 2.4 \times 10^{-2}\ s.$$

This value is much shorter than the experimentally determined value of $t_{min} = 20.4$ s. Consequently, reaction (III) is not diffusion controlled. This is also evidenced by the results of measurements of the rate constant of reaction (I) ($T = 295$ K, $P_{H_2} = 1.5$ Torr; see above). In this experiment, a decrease in the concentration of radicals (I) by a factor of 10 did not cause a noticeable decrease in the concentration of carbon-centered radicals (II) (changes were no higher than a few percents); that is, the lifetime of these radicals was longer than 10^3 s under these conditions, whereas in the diffusion-controlled reaction it would be

$$t_D = (k_D(295\ K)\,P'_{H_2})^{-1}$$
$$= (4\pi r_0 D(295\ K)\,P'_{H_2})^{-1}$$
$$= (4\pi(5 \times 10^{-8})(1.1 \times 10^{-11}) \times (1.46 \times 10^{15}))^{-1} = 1 \times 10^2\ s.$$

To estimate the activation energies E_{min} and E_{max}, we should specify preexponential factors. Assuming that they are the same for various radical groups, at $k_0 = 1 \times 10^{-11}\ cm^3\ molecule^{-1}\ s^{-1}$, $E_{min} = 10$ kcal/mol and $E_{max} = 17.4$ kcal/mol.[2] Hence, the average activation energy is $E_{av} = 14$ kcal/mol. The estimated height of an activation barrier seems reasonable. For the thermally neutral reactions of this kind, the activation energy is 11–14 kcal/mol [21]. It can be somewhat higher for the endothermic test reaction (the strengths of C–H and H–H bonds are about 100 and 104 kcal/mol, respectively) (the Polanyi–Semenov rule).

[2] At $k_0 = 1 \times 10^{-12}\ cm^3\ molecule^{-1}\ s^{-1}$, we obtain $E_{min} = 7$ kcal/mol and $E_{max} = 14.5$ kcal/mol. The activation barrier of 7 kcal/mol for the reaction occurring under kinetic control, the activation energy of 10.4 kcal/mol for the diffusion of hydrogen molecules, seems underestimated.

Figure 7b shows the kinetic curve of the decay of radicals reacting with the rate constant $k = 1 \times 10^{-11}\exp(-14\ (\text{kcal/mol})/RT)$ at $T = 650$ K and $P_{H_2} = 2.5 \times 10^{-2}$ Torr. The activation energy was specially chosen to be the same as the average activation energy of the stepwise process $E = E_{av} = 14$ kcal/mol. At this choice, both of the kinetic curves afforded the same reaction halftimes; however, noticeable differences in the regions of small and, especially, high degrees of conversion were observed.

Let us consider the degradation reactions of the hydrogenation products of the test radicals. The exposure of RSi samples in an atmosphere of H_2 (0.2 Torr) at 875 K and their cooling in an atmosphere of hydrogen to room temperature resulted in the complete decay of $(\equiv Si-)_3C^{\bullet}$ and $(\equiv Si-O-)_3Si^{\bullet}$ PMCs (Fig. 8, spectrum *1*). The pyrolysis of a hydrogenated sample was accompanied by the formation of low-molecular-weight degradation products (mainly, molecular hydrogen), which were removed from the system by pumping (to a pressure of $<10^{-4}$ Torr). The process was accompanied by an increase in the concentration of PMCs in the sample. Figure 8 shows the EPR spectra of the dehydrogenation products obtained at various pyrolysis temperatures (the exposure time at each particular temperature was 10 min). They are a superposition of the EPR signals of $(\equiv Si-)_3C^{\bullet}$ (a single line with a g factor of 2.0026) and $(\equiv Si-O-)_3Si^{\bullet}$ radicals (an anisotropic signal with an axially symmetrical g tensor: $g_{||} = 2.0018, g_{\perp} = 2.0003$) (Fig. 8, spectra *2*–*4*). Thus, pyrolysis was accompanied by the degradation of Si–H and C–H bonds and the regeneration of PMCs. The cycle of the decay of $(\equiv Si-)_3C^{\bullet}$ and $(\equiv Si-O-)_3Si^{\bullet}$ radicals in an atmosphere of hydrogen and their reduction upon high-temperature vacuum heating (reactions (I)–(IV)) can be performed several times without a considerable change in the concentration of free radicals. The $(\equiv Si-)_3C^{\bullet}$ and $(\equiv Si-O-)_3Si^{\bullet}$ radicals in RSi samples were stable at the temperatures of the homolytic cleavage of $(\equiv Si-)_3C-H$ and $(\equiv Si-O-)_3Si-H$ bonds. Therefore, in the presence of $H_2(D_2)$ molecules, they can play the role of a generator of atomic hydrogen (deuterium) in silica. The ratio between the amounts of the resulting two types of radicals changed only slightly in the course for pyrolysis (see Fig. 8), although it covers a wide range of temperatures. For this purpose, the activation energies of the reactions of C–H and Si–H bond cleavage should be close (differ by no more than 2–3 kcal/mol). Because the reverse reactions of radical combination with H atoms occur with no activation, the strengths of these bonds in the groups under consideration are similar (the results of model quantum-chemical calculations provide support to this conclusion, see Table 2).

5. Simulation of the kinetics of the processes. The experimental results suggest the nonequivalence of the spectroscopic and kinetic characteristics of individual groups of PMCs stabilized in an amorphous silica matrix. These differences are due to their spatial structures. Data on the relationships between these characteristics of reacting species can be obtained using quantum chemistry. The accepted model should take into consideration the effect of a surrounding matrix on relaxation processes, which always accompany chemical transformations occurring in the system. It also should make it possible to vary the spatial structure of a center. We used the $(\equiv Si-)_3C^{\bullet}$ radical as a model of the $(F_3Si-)_3C^{\bullet}$ PMC. The matrix effect on the structural rearrangements of reactants in the course of a chemical reaction was simulated by fixing the spatial arrangement of atoms that constitute the $(F_3Si-)_3$ group. The structural disorder of amorphous silica was simulated by varying the geometric structure of the radical. The calculations were performed for the following processes:

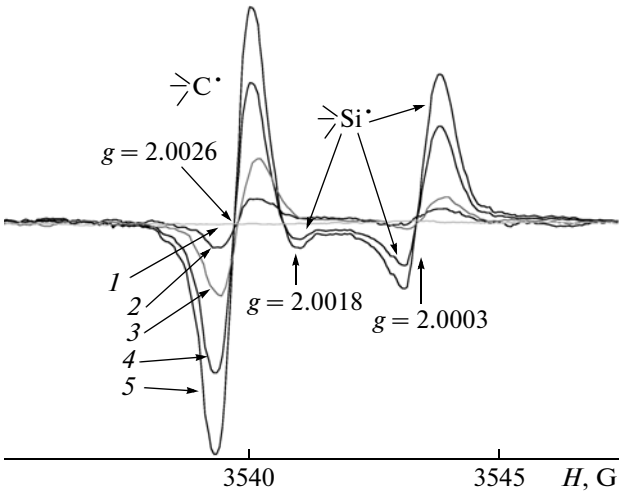

Fig. 8. EPR spectra of PMCs formed upon the thermal degradation of groups $(\equiv Si-O-)_3Si-H \longrightarrow (\equiv Si-O-)_3Si^{\bullet} + H$, $(\equiv Si-)_3C-H \longrightarrow (\equiv Si-)_3C^{\bullet} + H$.

Reaction temperature, K: (*1*) 1450, (*2*) 1300, (*3*) 1150, (*4*) 1000, or (*5*) 850.

Exposure, 10 min at each temperature. The EPR signals were detected at 300 K.

$$(F_3Si-)_3C^{\bullet} + H_2 \longrightarrow TS \longrightarrow (F_3Si-)_3CH + H,$$

$$(F_3Si-)_2C^{\bullet}H + H_2 \longrightarrow TS \longrightarrow (F_3Si-)_2CH_2 + H,$$

$$(F_3Si-)C^{\bullet}H_2 + H_2 \longrightarrow TS \longrightarrow (F_3Si-)CH_3 + H,$$

$$F_3Si^{\bullet} + H_2 \longrightarrow TS \longrightarrow F_3Si-H + H.$$

Using the first reaction as an example, we attempted to simulate the effects of spectral and kinetic nonequivalence, which were experimentally found for $(\equiv Si-)_3C^{\bullet}$ radicals. Therefore, we performed calculations for radicals $(F_3Si-)_3C^{\bullet}$ (*A*), in which they had specially chosen spatial forms *A*(0), *A*(1), and *A*(2). For a portion of atoms in their structure, their spatial positions were fixed and remained unchanged in the course of all of the subsequent calculations. The structure of *A*(1) was obtained from the

Table 2. Results of the quantum-chemical calculations (DFT/B3LYP//6-311G**) of the characteristics of the processes $Z^{\bullet} + H_2 \longrightarrow TS \longrightarrow Z{-}H + H$ (for $Z^{\bullet} = (F_3Si{-})_3C^{\bullet}$, three different spatial structures of the coordination sphere of the carbon atom were used (see the text))

Entry	$Z^{\bullet}$	<XCSi*, φ, deg	$a_{\parallel}(^{13}C)$, G	E_{act}^{***}, kcal/mol	<HCSi, φ, deg	ν(Z–H) **, cm^{-1}	Q(Z–H)***, kcal/mol
1	$(F_3Si{-})_3C^{\bullet}$(*A*(0))	90	66.9	**14**(11.2)	105.4	3012	**100.8**(97.8)
2	$(F_3Si{-})_3C^{\bullet}$(*A*(1))	90	66.9	**17**(13.1)	98.7	2943	**98**(94.6)
3	$(F_3Si{-})_3C^{\bullet}$(*A*(2))	99.5	86.4	**12**(8.4)	105.4	3012	**104**(100.7)
4	$(F_3Si{-})_2C^{\bullet}H$		70.4	**15**(11.5)		3043(2.4) 3090(2.0)	**101.6**(98.4)
5	$(F_3Si{-})C^{\bullet}H_2$		75.0	**14.3**(11.1)		3045(0) 3121(4.2)	**104.0**(99.9)
6	$F_3Si^{\bullet}$	115.7	–	**12.9**(9.2)	111.0	2373(68)	**100.1**(97.2)

*In entry 6, the <XSiF and <HSiF bond angles are given.

**Line intensities (km/mol) are given in parentheses (after vibration frequencies).

***The results of calculations at the G2(MP2) level are boldfaced, and the results of calculations at the DFT level are given in parentheses.

equilibrium structure of the $(F_3Si{-})_3C^{\bullet}$ radical *A*(0) with the fixation of the positions of all of the atoms other than carbon (of course, the C atom occupied its equilibrium position in this case). The radical structure of *A*(2) was derived from the equilibrium structure of the $(F_3Si{-})_3C^{\bullet}{-}H$ group by fixing the positions of all atoms other than C and H in it, removing the H atom, and optimizing the position of the C atom. In all of the subsequent calculations, only C and H atoms could freely move. The above structures were chosen no randomly: *A*(1) and *A*(2) characterize the width of the distribution function due to possible differences in the spatial structures of defects in a disordered solid. In a manner, they are an analog of the values of k_{min} and k_{max}, which are responsible for the form of the distribution function of the number of particles in terms of the rate constants of their conversion, when they are kinetically nonequivalent. The easiest and the most difficult ways from a radical to the product of H-atom addition are related to the structures of *A*(1) and *A*(2). The relationship between these two distributions can be found using quantum chemistry.

Table 2 summarizes the results of the calculations. It contains the characteristics of starting reactants (the first three columns), activation energies for the reaction of H-atom abstraction from the H_2 molecule by a radical (transition state energies, the fourth column), and data on the reaction product Z–H (its geometry, the frequency of the stretching vibration of the Z–H bond, and the strength of the Z–H bond). The results given in Table 2 were obtained using calculations at the DFT level (figures in parentheses). The refinement of the energies of individual structures at the G2(MP2) level resulted in an increase in the height of activation barriers and the strengths of C–H and Si–H bonds by 3–3.5 kcal/mol (boldfaced).

The kinetic characteristics of the hydrogenation reaction of radical $(F_3Si{-})_3C^{\bullet}$ depend on its spatial structure (Table 2, 1–3). In Section 3, we demonstrated that $(\equiv Si{-})_3C^{\bullet}$ radicals differ in the HFC constants of an unpaired electron with the ^{13}C nucleus ($a_{\parallel}(^{13}C)$), which lie in a range from 69.5 to 87.5 G. The value of this constant reflects the electronic state of the carbon atom, which, in turn, is controlled by the spatial structure of the radical and is responsible for its reactivity. These constants are 66.9 and 86.4 G for radicals *A*(1) and *A*(2); that is, they vary in approximately the same range (see Table 2). This result suggests that the scales of the spatial structure changes of radicals in the RSi sample and model structures *A*(1) and *A*(2) used in the calculations are close to each other. This similarity manifests itself in the reaction kinetics of the hydrogenation of $(F_3Si{-})_3C^{\bullet}$ and $(\equiv Si{-})_3C^{\bullet}$ radicals. The $(\equiv Si{-})_3C^{\bullet}$ PMCs, which participate in this simple chemical reaction that occurs in an amorphous solid, are kinetically nonequivalent, and the activation energies of their reactions with hydrogen molecules are distributed over a range from 10 to 17.4 kcal/mol (the average value of 13.7 kcal/mol). According to the results of calculations, the activation energies of the hydrogenation reactions of structures *A*(1) and *A*(2) are 17 and 12 kcal/mol, respectively, with the average value of 14.5 kcal/mol (Table 2). This average value is close to a barrier of 14 kcal/mol for the free mode (Table 2, entry 1; structure *A*(0)) of this reaction. Thus, the model proposed reflects the main peculiarities of the above solid-phase processes—the characteristic parameters and the scales of differences due to a disordered solid structure.

In accordance with experimental data, the calculations demonstrated that, among the PMCs summarized in Table 2, the $(F-)_3Si^{\bullet}$ radicals, the models of $(\equiv Si-O-)_3Si^{\bullet}$ centers in silica, exhibited the highest chemical activity toward hydrogen. The activation energy of hydrogen atom abstraction calculated for these radicals is 12.9 kcal/mol (the experimental value for $(\equiv Si-O-)_3Si^{\bullet}$ radicals is 11.2 kcal/mol, and a broad reaction rate constant distribution was not found for this reaction). According to the results of calculations, carbon-centered radicals of different types (see Table 2) have the similar activation barriers for the hydrogenation reaction, which are 14–15 kcal/mol, that is, ~2 kcal/mol higher than that for silicon-centered radicals.

The strength of the C–H and Si–H bonds formed as a result of hydrogenation is about 100 kcal/mol. However, in the case of $(\equiv Si-)_3C^{\bullet}$ PMCs, as a consequence of their kinetic nonequivalence, a strength distribution of the resulting C–H bonds (possibly, to 10 kcal/mol, Table 2) would be expected. The reactivity of individual groups of $(\equiv Si-)C^{\bullet}H_2$ radicals having a labile CH_2 group should be similar. In this series, $(\equiv Si-)_2C^{\bullet}H$ radicals occupy an intermediate position—they do not contain labile fragments, but the presence of the H atom as a substituent at the carbon atom allows this latter to alter (change its hybridization) in the course of a chemical reaction.

6. The nature of EX centers in oxidized silicon samples. In the oxidation products of silicon (single crystal plates [22] and porous silicon [23, 24], an EPR signal from PMCs was detected. This signal was similar in characteristics to the spectrum of $(\equiv Si-)_3C^{\bullet}$ radicals in RSi samples containing natural amounts of isotopes. It was a narrow single line with $g = 2.00246$ and two satellites, the total intensity of which was about 15% of the total intensity of the EPR signal, and the doublet splitting was 16.1 G (only samples with the naturally occurring concentrations of the magnetic isotopes of the elements were used). Stesmans [22] also found that centers reacted with molecular hydrogen: they decayed in an atmosphere of H_2, whereas they were regenerated upon high-temperature vacuum heating. The defect was referred to as an EX center [22]. It was assumed [22–24] that the PMC is an intrinsic defect of SiO_2, and it is a hole center arranged at the site of a silicon vacancy, in which an unpaired electron was delocalized among three or four neighboring oxygen atoms. However, a particular model for the center was not proposed.

The similarity of the spectral (radiospectroscopic) characteristics and chemical properties of EX centers and $(\equiv Si-)_3C^{\bullet}$ radicals (see Sections 3 and 4) suggests that both of them are the same carbon-centered PMC in SiO_2, whose first coordination sphere of the C atom consists of three magnetically equivalent silicon atoms: $(\equiv Si-)_3C^{\bullet}$.

7. Probable mechanism of the incorporation of carbon into the silica structure. The source of carbon as a constituent of RSi samples is the methoxy group $\equiv Si-O-CH_3$, in which the silicon and carbon atoms are separated by oxygen. The main channel of the thermal transformation of these groups is decomposition with the elimination of a formaldehyde molecule and the formation of a Si–H bond [2–6]:

$$\equiv Si-O-CH_3 \longrightarrow \equiv Si-H + CH_2 = O. \qquad (V)$$

The removal of an oxygen atom from the coordination sphere of the lattice silicon atom is a key step in the preparation of RSi, an oxygen-deficient silica sample. The strength of the formed Si–H bond (about 100 kcal/mol) is lower than the strength of the Si–O bond (≈140 kcal/mol [8]), and the homolytic cleavage of a hydride with the formation of a silyl radical and a hydrogen atom becomes possible at temperatures of ≈1000 K [8]:

$$\equiv Si-H \longrightarrow \equiv Si^{\bullet} + H. \qquad (VI)$$

The formation of RSi occurs with the participation of this free-radical species.

The $\equiv Si-CH_3$ and $\equiv Si-OH$ groups (with absorption bands at 2983 and 3746 cm^{-1}, respectively [4, 25]) were detected in the thermal degradation products of methoxy groups by IR spectroscopy along with hydrides (Si–H) at the initial stage of the preparation of RSi (900–1000 K). The appearance of $\equiv Si-{}^{\bullet}CH_2$ radicals in the same samples was detected by EPR spectroscopy (see Section 1). After heating a sample at 1100–1200 K, methyl radicals and, simultaneously, $\equiv Si-{}^{\bullet}CH_2$ radicals disappeared. Therefore, the $\equiv Si-CH_3$ groups are precursors for $\equiv Si-{}^{\bullet}CH_2$ radicals. Because the strengths of C–H and Si–H bonds are similar (see Sections 4 and 5), a carbon-centered radical can be formed in both reaction (VII) with the H atom, which is a product of Si–H bond cleavage (reaction (VI)), and as a result of the thermal degradation of a C–H bond in a hydrocarbon radical (reaction (VIII)):

$$\equiv Si-CH_3 + H \longrightarrow \equiv Si-{}^{\bullet}CH_2 + H_2; \qquad (VII)$$

$$\equiv Si-CH_3 \longrightarrow \equiv Si-{}^{\bullet}CH_2 + H. \qquad (VIII)$$

As the pyrolysis temperature was increased, new types of PMCs, $(\equiv Si-)_2{}^{\bullet}CH$ and $(\equiv Si-)_3C^{\bullet}$, were stabilized in the sample. The hydrogenation of $(\equiv Si-)_3C^{\bullet}$ in an atmosphere of H_2 and the reverse reaction of thermal regeneration are considered in Section 4; they occur in accordance with the same scenario. Thus, the series of carbon-centered PMCs—$\equiv Si-{}^{\bullet}CH_2$, $(\equiv Si-)_2{}^{\bullet}CH$, and $(\equiv Si-)_3C^{\bullet}$—have the diamagnetic groups $\equiv Si-CH_3$, $(\equiv Si-)_2CH_2$, and $(\equiv Si-)_3CH$ as their precursors, respectively. Both the diamagnetic and paramagnetic series of centers are the products of the consecutive steps of carbon insertion into the silica lattice (the replacement of a C–H bond by C–Si):

$$\equiv Si^{\cdot}CH_2 + {}^{\cdot}Si\equiv \longrightarrow (\equiv Si-)_2CH_2, \quad (IX)$$

$$(\equiv Si-)_2CH_2 + H \longrightarrow (\equiv Si-)_2{}^{\cdot}CH + H_2, \quad (X)$$

$$(\equiv Si-)_2CH_2 \longrightarrow (\equiv Si-)_2{}^{\cdot}CH + H, \quad (XI)$$

$$(\equiv Si-)_2{}^{\cdot}CH + {}^{\cdot}Si\equiv \longrightarrow (\equiv Si-)_3CH, \quad (XII)$$

$$(\equiv Si-)_3CH + H \longrightarrow (\equiv Si-)_3{}^{\cdot}C + H_2, \quad (XIII)$$

$$(\equiv Si-)_3CH \longrightarrow (\equiv Si-)_3{}^{\bullet}C + H, \quad (XIV)$$

$$(\equiv Si-)_3{}^{\cdot}C + {}^{\cdot}Si\equiv \longrightarrow (\equiv Si-)_4C. \quad (XV)$$

A necessary participant of this process, which is completed by the formation of $(\equiv Si-)_4C$ groups, is a silyl radical, the product of reaction (VI).

The amount of dissolved carbon atoms in the RSi samples was determined experimentally. The heating of the RSi sample in an atmosphere of oxygen (P_{O_2} = 0.1–1 Torr) at 1150 K resulted in the consumption of $(1.2 \pm 0.1) \times 10^{13}$ cm^{-2} oxygen molecules and the formation of $(0.7 \pm 0.1) \times 10^{13}$ cm^{-2} CO_2 molecules (0.5–0.7 per chemisorbed molecule of O_2). The ratio between the amount of chemisorbed oxygen and the number of formed CO_2 molecules indicates that oxygen was mainly consumed with the participation of carbon-containing groups—the conversion of C into CO_2 plus the oxidation of liberated silicon atoms:

$$((\equiv Si-O-)_3Si-)_4C + O_2$$
$$\longrightarrow ((\equiv Si-O-)_3Si-)_2C=O + ((\equiv Si-O-)_3Si-)_2O;$$
$$O((\equiv Si-O-)_3Si-)_2C = O + O_2$$
$$\longrightarrow ((\equiv Si-O-)_3Si-)_2O + CO_2.$$

Thus, the major portion of dissolved carbon in RSi samples enters into the composition of diamagnetic groups. Among these groups, $(\equiv Si-)_4C$ is the most stable. These groups are the main carriers of carbon at the final stages of the formation of RSi.

Reactions (VII)–(XV) represent the process of carbon incorporation into the structure of silica, which is started at the $\equiv Si-CH_3$ group. What is the mechanism of the formation of this group?

Ing et al. [26] performed quantum-chemical calculations and found that the methanol molecule has two channels of degradation whose products are (formaldehyde + hydrogen) and (carbene + water). The difference between the activation barriers of these processes (88 and 92 kcal/mol, respectively) is 4 kcal/mol. Does the methoxy group have a second channel of degradation in addition to that leading to the formation of a formaldehyde molecule and a Si–H group? The following reaction scheme shows the results of the calculation of the activation energies of two degradation channels of the $F_3Si-O-CH_3$ molecule, which is the model of the methoxy group at the surface of silica (calculation at the G2(MP2)/B3LYP//6-311G** level):

$$F_3Si-O-CH_3$$
$$\longrightarrow F_3Si-O-H + :CH_2, E_a = 87 \text{ kcal/mol},$$
$$F_3Si-O-CH_3$$
$$\longrightarrow F_3Si-H + O=CH_2, E_a = 84 \text{ kcal/mol}.$$

Differences between the activation energies of the two transformation channels of the methoxy group differ only slightly from those obtained for the methanol molecule [26]. Therefore, at T = 1000 K, about 10% of reaction products must be carbene molecules (at the same values of preexponential factors for rates constants of these reactions).

With consideration for the high activity of carbenes in insertion reactions, it is believed that their reaction with Si–H groups on the surface of RSi results in the formation of methyl–silyl groups:

$$\equiv Si-O-CH_3 \longrightarrow \equiv Si-O-H + :CH_2, \quad (XVI)$$

$$\equiv Si-H + :CH_2 \longrightarrow \equiv Si-CH_3. \quad (XVII)$$

Both of the products of these reactions ($\equiv Si-O-H$ and $\equiv Si-CH_3$ groups) were detected by IR spectroscopy at the early stages of the formation of the RSi structure [4, 25].

Thus, the hypothesis [25] on the carbene mechanism of the formation of methyl–silyl groups on the surface of RSi does not contradict available results of experimental and quantum chemical studies.

ACKNOWLEDGMENTS

This study was supported by the Russian Foundation for Basic Research (project nos. 07-02-00955-a, 09-02-12325-ofi-m, 09-03-00475-a, and 10-03-00909-a) and the 01-OKhNM Program "Theoretical and Experimental Studies of the Nature of Chemical Bonds and the Mechanisms of the Most Important Chemical Reactions and Processes" of the Russian Academy of Sciences.

REFERENCES

1. Worhoff, K., Lambeck, P.V., and Driessen, A., *J. Lightwave Technol.*, 1999, vol. 17, no. 8, p. 1401.
2. Morterra, C. and Low, M.J.D., *J. Chem. Soc., Chem. Commun.*, 1968, p. 203.
3. Morterra, C. and Low M.J.D., *Ann. N. Y. Acad. Sci.*, 1972, vol. 220, p. 135.
4. Morterra, C. and Low, M.J.D., *J. Phys. Chem.*, 1969, vol. 73, p. 321.
5. Radtsig, V.A., *Chem. Phys. Rep.*, 1995, vol. 14, no. 8, p. 1206.
6. Radzig, V.A., in *Defects in SiO_2 and Related Dielectrics: Science and Technology*, Pacchoini, G., Skuja, L., and Griscom, D.L., Eds., Dordrecht: Kluwer, 2000, p. 339.
7. *Gaussian 94, Revision D.1*, Frisch, M.J., Trucks, G.W., Schlegel, H.B., Gill, P.M.W., Johnson, B.G., Robb, M.A., Cheeseman, M.A., Keith, T., Petersson, G.A., Montgomery, J.A., Raghavachari, K., Al-Laham, M.A.,

Zakrzewski, V.G., Ortiz, J.V., Foresman, J.B., Cioslowski, J., Stefanov, B.B., Nanayakkara, A., Challacombe, M., Peng, C.Y., Ayala, P.Y., Chen, W., Wong, M.W., Andres, J.L., Replogle, E.S., Gomperts, R., Martin, R.L., Fox, D.J., Binkley, J.S., Defrees, D.J., Baker, J., Stewart, J.P., Head-Gordon, M., Gonzalez, C., and Pople, J.A., Pittsburgh, Penn.: Gaussian Inc., 1995.

8. Radzig, V.A., in *Thin Films and Nanostructures*, Trakhtenberg, L.I., Lin, S.H., and Ilegbusi, O.J., Eds., Amsterdam: Elsevier, 2007, vol. 34, p. 233.
9. Becke, A.D., *J. Chem. Phys.*, 1993, vol. 98, p. 5648.
10. Lee, C., Yang, W., and Parr, R.G., *Phys. Rev. B: Condens. Matter*, 1988, vol. 37, p. 785.
11. Curtiss, L.A., Raghavachari, K., and Pople, J.A., *J. Chem. Phys.*, 1993, vol. 98, no. 2, p. 1293.
12. Radtsig, V.A., *Khim. Fiz.*, 2000, vol. 19, no. 3, p. 17.
13. Pshezhetskii, S.Ya., Kotov, A.G., Milinchuk, V.K., Roginskii, V.A., and Tupikov, V.I., *EPR svobodnykh radikalov v radiatsionnoi khimii* (ESR of Free Radicals in Radiation Chemistry), Moscow: Khimiya, 1972.
14. Bobyshev, A.A. and Radtsig, V.A., *Khim. Fiz.*, 1986, vol. 5, p. 911.
15. Radtsig, V.A. and Bystrikov, A.V., *Kinet. Katal.*, 1978, vol. 19, p. 713.
16. Lebedev, Ya.S. and Muromtsev, V.I., *EPR i relaksatsiya stabilizirovannykh radikalov* (EPR and Relaxation of Stabilized Radicals), Moscow: Khimiya, 1972.
17. Bobyshev, A.A., Radtsig, V.A., and Senchenya, I.N., *Kinet. Katal.*, 1990, vol. 31, no. 4, p. 931.
18. Mikhailov, A.I., Lebedev, Ya.S., and Buben, N.Ya., *Kinet. Katal.*, 1964, vol. 5, no. 6, p. 1020.
19. Radtsig, V.A., *Vysokomol. Soedin., Ser. A*, 1975.
20. Shelby, J.E., *J. Appl. Phys.*, 1977, vol. 48, no. 8, p. 3387.
21. Benson, S.W., *The Foundations of Chemical Kinetics*, New York: McGraw-Hill, 1960.
22. Stesmans, A., *J. Non-Cryst. Solids*, 1994, vol. 179, p. 10.
23. Carlos, W.E. and Prokes, S.M., *J. Appl. Phys.*, 1995, vol. 78, no. 3, p. 2129.
24. Prokes, S.M. and Carlos, W.E., *J. Appl. Phys.*, 1995, vol. 78, no. 4, p. 2671.
25. Permenov, D.G., *Cand. Sci. (Chem.) Dissertation*, Moscow: Inst. of Chemical Physics, 2005.
26. Ing, W.C., Sheng, C.I., and Bozzelli, J.W., *Fuel Process. Technol.*, 2003, vol. 83, p. 111.